Pre-processing Methods for Change Detection on Under-sampled and Noisy Fourier Data

A Thesis Presented in Partial Fulfillment of

the Honors Bachelor's Degree

Ivy Junqing Yan

Abstract

In this project we present a new algorithm to detect changes multiple scenes given a time sequence of Fourier data. The algorithm incorporates an edge detection method that uses the Fourier data directly. This is beneficial in applications when recovering an accurate sequence of images is not possible, for example when the data acquisition is compromised in some way, which could happen as a result of obstruction or significant noise. In such cases, recovering the edges of each image may be more feasible. Here we explore the effects of using edge information that is obtained from under-sampled Fourier data, specifically when bands of Fourier data are missing in each of the data collections which prevents accurate reconstruction of the underlying images. We demonstrate that in this case, having an accurate edge map will still allow us to determine change in the sequence of images.

Department of Mathematics

Under the supervision of Professor Anne Gelb

Dartmouth College

May 2022

Contents

List of Figures

List of Tables

Acknowledgments

I would like to thank Professor Anne Gelb for her endless dedication to me personally and to the project. She believed in me from the very start and was a big supporter for women in mathematics. She taught me to be curious and to love to learn; things that will carry with me beyond school and college. Thank you to all the professors and staff from the department of Mathematics and thayer school of engineering for the support.Thank you to Jack Zhang and Will Kaufman, and all the friends that was a part of making this happen.

1 Introduction

Change detection is the ability to recognize differences between images that are observed at different times. Researchers are interested in fast and accurate change detection results in analyzing Fourier data. This operation has wide applications in areas such as MRI to help monitor patient health or radar images in monitoring land changes for environmental researches. Change detection algorithms can be largely separated into two categories: "online change detection" and "offline change detection." Online change detection refers to algorithms that focuses on detecting changes in an on-going stream of data and is mostly done with Bayesian methods or streaming algorithms [2]. This paper focuses on the second category, offline change detection, which refers to detecting changes on already observed time series. While advanced and robust methods have been developed for change detection given Fourier data [2], such algorithms require accurate reconstruction of inputs in the spatial domain. Fourier reconstruction is fundamental in operating many sensing devices and is integral to signal and system analysis. After devices collect signals in the frequency domain an inverse Fourier transform is employed, allowing us to decipher and analyze information from data collected. Fourier signals have far reaching applications in all branches of engineering and sciences, particularly electrical engineering. Fourier data has a wide range of applications, including the use of ultrasound devices, magnetic resonance imaging (MRI), synthetic aperture radar (SAR) and more [3].

However, when we obtain compromised Fourier data, the accuracy of such reconstruction process drastically decreases. Such situations may occur when sensors have limited band width or when certain frequency bands are interfered. This thesis will specifically focus on the collection of Fourier data for $2D$ images, specifically when the data is noisy and under-sampled. We want to detect changes on sequences of images collected as Fourier data at different times. Current literature to improve accuracy of change detection focuses on increasing the rigorousness of image reconstruction. Methods to reconstruct image from under-sampled data are described in [1] and [12]. These methods could become computational costly when the scale of the problem gets large. We seek to develop a pre-processing

method using concentration factor to detect changes. Concentration factors allow us to obtain an edge map on these images, by-passing a reconstruction need completely.

We have discovered that a robust reconstruction is not necessary to yield accurate results. We conjectured that it could be beneficial to recover an edge map of the original images in order to obtain an accurate change detection. The goal is to keep the results of change detection robust even in absence of full bands of Fourier data. This investigation focuses on devising a pre-processing method for the generalized likelihood ratio test, (GLRT), a commonly used statistical change detection algorithm [8]. As will be demonstrated in our numerical results, our pre-processing method using the concentration factor edge detection method [5], a method to obtain an edge map directly from Fourier data, improves the output of GLRT in case of under-sampled Fourier data. Moreover, our method is computationally efficient since it is achieved without individual image reconstruction.

The rest of the thesis is organized as follows. Section two describes and defines the problem set up; section three introduces our new method and discuss in detail all components of the algorithm; numerical experiments are provided in section four; conclusion and on-going investigations are described in section five.

2 Problem Formulation and Data

2.1 Problem Formulation

For simplicity, we assume the signals we acquired are all real valued. Let $f(x, y) \in [0, 1]^2$ be the spatial representation of the underlying signal. The function is sparse in edge domain and is of size $N \times N$, $f(x, y) \in [0, 1]$ where $f(x, y)$ represents pixel value at location (x, y). The following figure shows an example of the true function:

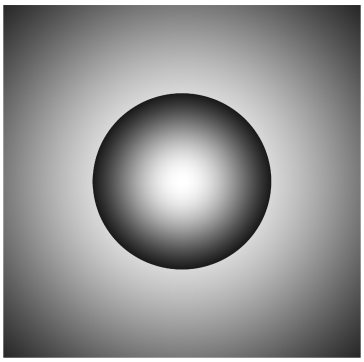

Figure 1: Underlying Scene

We then apply a change to the underlying scene. In the following data, the change magnitude is 0.8 and the change square is sized at 12×12 pixels.

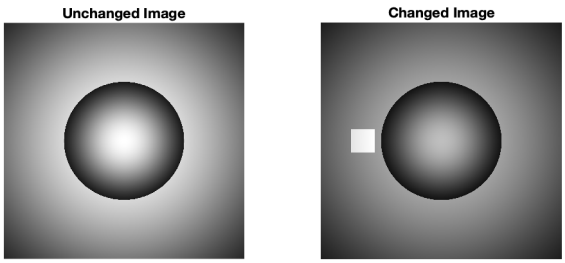

Figure 2: Changed VS. Unchanged Image

The image is then approximated into a Fourier signal following definition 2.1 below:

Definition 2.1. Given an image in the spatial domain, $f(x, y)$, of size $N \times M$, the Fourier transform of $f(x, y)$, namely, $F(u, v)$, is defined as

$$F(u, v) = \int_0^1 \int_0^1 e^{-i2\pi(ux/N+vy/M)} f(x, y)dxdy \tag{1}$$

and the inverse Fourier transform of $F(u, v)$ is defined as

$$f(x, y) = \frac{1}{NM} \sum_{u=0}^{N-1} \sum_{v=0}^{M-1} e^{i2\pi(ux/N+vy/M)} F(u, v) \tag{2}$$

The Fourier transform and inverse Fourier transforms are both implemented with built in Fast Fourier Transform (FFT) functions in MATLAB. Note that the true Fourier transform with integral definition is analytically difficult to compute. We simulate the integration by over-sampling the image, and then use the over-sampled point with partial sum approximation to achieve the integral set up.

$$F(u, v) = \int_0^1 \int_0^1 e^{-i2\pi(ux/N+vy/M)} f(x, y)dxdy,$$

By an over-sampled partial sum and we assume such Fourier signal, $F(u, v)$, will be the input of our experiments. In the following initial explorations, we simply took the inverse Fourier transform, also described in Definition 2.1, as reconstruction. Since no noise or any additional information loss occurs at this stage, the reconstruction is identical to the original images shown above. Given the robust reconstruction of images, a statistical change detection yields accurate results as seen below in figure 3

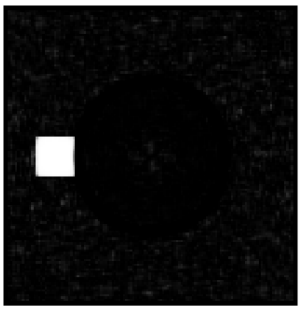

Figure 3: Change Characteristic of Un-compromised Data

Using a likelihood ratio test devised by Novack in [8], we can see the change characteristics displayed above accurately captures the change in the images.

Now consider the same images with bands of frequency zeroed out. For this initial investigation, we have blocked out channels of width 15 in the Fourier domain for each of the image in our collected data. The masks are applied so that each of the input data have non-overlapping compromised channels. We denote the compromised Fourier signal as F^*. For the J^{th} image, the missing bands are defined as :

$$F_J^*(u,v) = 0 \text{ for } 15J \leq u \leq 15(J+1)$$

i.e. Image 1 has pixel 1 to 15 masked; image 2 has pixel 15 to 30 blocked and this pattern continues. The accuracy of the reconstruction using inverse Fourier transform is clearly affected by these missing bands of data.

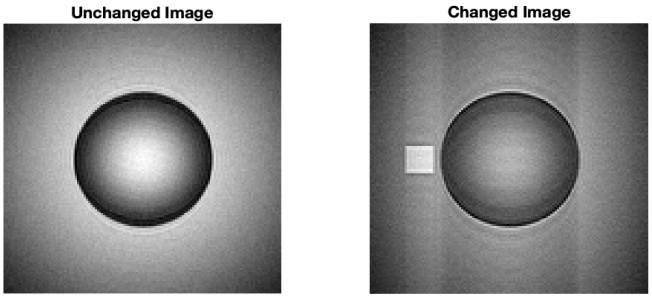

Figure 4: Changed VS. Unchanged Image of Compromised Data

Such compromised reconstruction now affects the accuracy of statistical change detection as seen in figure 5 below:

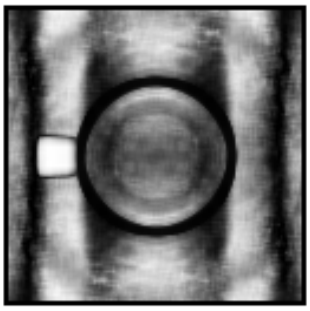

Figure 5: Change Characteristic of Compromised Data

We then employed the concentration factor edge detection method, which allows us to detect edges directly from the Fourier data, bypassing a rigorous reconstruction. The concentration factor method, which is described in details in Section 3, acts essentially as a band-pass filter. This results in the reconstruction focusing on the singular support of the underlying piece-wise smooth signal. Figure 6 shows the edge map constructed using the concentration

factor method when some of the Fourier bands are missing.

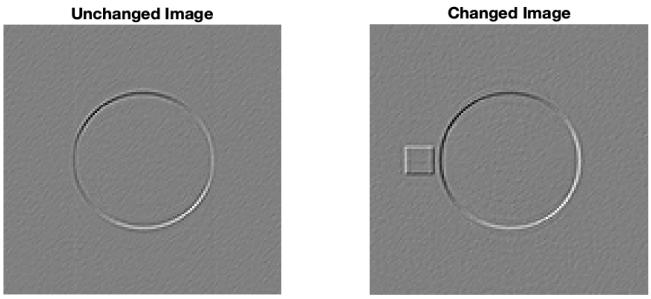

Figure 6: Edge Map of Compromised Data

For comparison purposes, Figure 7 shows the resulting edge map when no bands of Fourier data are missing.

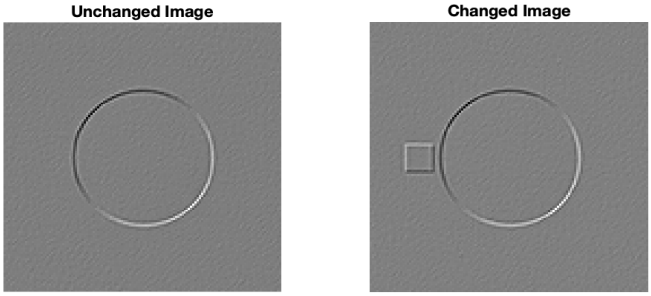

Figure 7: Edge Map of Original Data

We can see that the edge recovery remained accurate even in the less ideal case where Fourier bands are missing. This is in contrast to standard Fourier reconstruction, for which

the accuracy is greatly compromised in this case. Encouraged by these results, we are motivated to use the concentration factor edge detection method as a pre-processing method for statistical change detection. This will increase the accuracy results in situations of under-sampled Fourier data. Because of concentration factor method's ability to accurately recover edges from Fourier data, even when under-sampled and noisy, as described in [9], we hypothesize that this method will yield an accurate and efficient outcome as shown in Section 5.

3 Methodology

3.1 Concentration Factor

We use the concentration factor edge detection method to compute the discontinuities in the underlying period and piece-wise-smooth image from its corresponding Fourier coefficients. More details of this method, including its convergence analysis can be found in [5]. We describe the method in $1D$. Although the method can be adapted for $2D$ problems, for simplicity in computation, we use a dimension-by-dimension approach in our 2D numerical experiments. Simply put, the concentration factor method in one dimension computes an approximation of the jump function from the first $2N+1$ Fourier series coefficient using a partial Fourier sum and Fourier space filter factors. More specifically, given a piece-wise analytic periodic function f on $[-\pi, \pi]$, we assume we are given the first $2N+1$ Fourier coefficients

$$\hat{f}(k) = \frac{1}{2\pi} \int_{-\pi}^{\pi} f(x) e^{-ikx} dx \tag{3}$$

We wish to recover the jump function of f, given by definition 3.1 below:

Definition 3.1 (Jump Function)**.** Let the right and left-land limits of the function, $f(x^+)$ and $f(x^-)$, be defined at every point x in the domain. The jump function associated with f and denoted by $[f]$ is defined as the difference between the right and left hand limits of the function at every point x; i.e.

$$[f](x) := f(x^+) - f(x^-) \tag{4}$$

Note that the jump function is only non-zero at jump locations.[1] If f has jump locations $\xi_i \in (-\pi, \pi)$, then we denote $[f](\xi_i)$ with the value of the jump at ξ_i. i.e. the jump function takes the value of the jump (positive or negative) at discontinuity locations.

By the celebrated Shannon-Nyquist sampling theorem, the original function f can be re-

[1] We use both 'edge' and 'jump' to describe a point of discontinuity in the underlying function or image.

constructed given the value of $\hat{f}$ on $\mathbf{Z}$. The partial Fourier series $S_N f$ has the property

$$S_N f = \sum_{n=0}^{N} \hat{f}(n) e^{inx} \longrightarrow f \text{ as } N \longrightarrow \infty \tag{5}$$

As derived in [4], if a periodic function has a simple jump discontinuity $\xi \in (-\pi, \pi)$, then the following relation between the Fourier coefficients and the jump function using integration parts is shown:

$$\begin{aligned} \hat{f(k)} &= \int_{-\pi}^{\pi} f(x) e^{-ikx} dx \\ &= \int_{-\pi}^{\xi^-} f(x) e^{-ikx} dx + \int_{\xi^+}^{\pi} f(x) e^{-ikx} dx \\ &= \frac{[f](\xi) e^{-ik\xi}}{in} + \int_{-\pi}^{\pi} f'(x) \frac{-in}{e^{-ikx}} \\ &\approx \frac{[f](\xi) e^{-ik\xi}}{in} + \mathcal{O}(\frac{1}{n^2}) \end{aligned} \tag{6}$$

The relationship in equation 6 can be extended for linear combination of jump discontinuities and for edges in 2D.

Therefore, given the first $2N + 1$ Fourier coefficient of a piece-wise-smooth function, the method described in [6] modifies the partial Fourier series in equation 5, so that it converges to the jump function. With that, we have the following definition for a concentration factor:

Definition 3.2 (Concentration Factor)**.** A concentration factor is any function

$$\sigma : [-1, 1] \longrightarrow \mathbf{C}$$

designed so that

$$S_N^{\sigma}[f](x) = \sum_{|k| \leq N} \hat{f}(k) \sigma(\frac{|k|}{N}) e^{ikx} \longrightarrow [f](x) \text{ as } N \longrightarrow \infty \tag{7}$$

The convergence properties of this partial sum approximation to the jump function depend on the choices of concentration factors: $\sigma(\eta) = \sigma(\frac{|k|}{N})$. As discussed in [4], these factor satisfy the following three conditions:

1. $\sum_{k=1}^{N} \sigma(\frac{k}{N}) sin(kx)$ is odd
2. $\frac{\sigma(\eta)}{\eta} \in C^2(0,1)$
3. $\int_{\epsilon}^{1} \frac{\sigma(\eta}{\eta} \longrightarrow -\pi$ for a small ϵ

We now define the concentration kernel as the following :

Definition 3.3 (Concentration kernel)**.** The concentration kernel C_N^σ is defined as

$$C_N^\sigma(x) = i \sum_{|k| \leq N} (k) sgn(k) \sigma(\frac{|k|}{N}) e^{ikx} \tag{8}$$

The partial sum approximation defined above for the jump function is a convolution of the concentration kernel C_N^σ with Fourier coefficients $\hat{f}$,

$$S_N^\sigma[f](x) = (f * C_N^\sigma)(x) \tag{9}$$

The conditions we have defined above ensure the kernel is odd, normalized, and smooth up to ϵ, to approximate the jump function. While there are a family of concentration factors to choose from, in this investigation we simply choose to use the exponential concentration factors, with the factor defined as

$$\sigma_E(\eta) = C\eta e^{(\frac{1}{\alpha\eta(\eta-1)})} \tag{10}$$

and we set the order $\alpha = 16$, where C is the normalizing constant defined as

$$C = \frac{\pi}{\int_{1/N}^{1-1/N} exp(\frac{1}{\alpha\tau(\tau-1)} d\tau)}$$

.

Finally, since it will be important in the case of missing Fourier bands, we define the jump response of a concentration factor in definition 3.4 below:

Definition 3.4. (Jump Response) The jump response associated with a concentration factor σ, denoted by $W_0^{\sigma,N}(x)$, is defined as the jump function approximation of the unit ramp as generated by the concentration sum.

$$W_0^{\sigma,N}(x) = S_N^{\sigma}[r](x) = \sum_{|k|\leq N} \hat{r}(k)\sigma(\frac{|k|}{N})e^{ikx} = \frac{1}{2\pi}\sum_{0<|k|\leq N} \frac{\sigma(\frac{|k|}{N})}{|k|}e^{ikx} \tag{11}$$

where r is the unit ramp function with

$$\hat{r}(k) = \begin{cases} \frac{1}{2\pi ik} & k \neq 0 \\ 0 & k = 0 \end{cases} \tag{12}$$

The jump response becomes important in our later discussion for improving the concentration factor design in cases of under-sampled Fourier data [4].

3.2 Change Detection

In our investigation, we employed the generalized likelihood ratio test for change detection [8]. Starting with a likelihood ratio test, defined as

$$\frac{f(X_1, \ldots X_n, X_{N+1}, \ldots, X_{2N}|H_0)}{f(X_1, \ldots, X_N|H_0)f(X_{N+1}, \ldots, X_{2N}|H_1)} \tag{13}$$

where X_j is the j^{th} image. There are "N" independent data vectors in each of the changed and unchanged measurement sets. Under the Null Hypothesis, "H_0", $C = C_1 = C_2$ where C_1 is time one data and C_2 is time two data. All $2N$ data vectors are characterized by the joint PDF given by

$$f(X_1, \ldots, X_N, X_{N+1}, \ldots, X_{2N}) = \frac{exp\{-tr[C_1^{-1}\sum_{i=1}^{2N} X_i X_i^*]\}}{\pi^{2Np}|C_1|^{2N}} \tag{14}$$

Under the alternative Hypothesis "H_1", $C_2 \neq C_1$ and the joint PDF of the $2N$ data vector given by

$$f(X_1,\ldots,X_N)f(X_{N+1},\ldots,X_{2N}) = \frac{exp\{-tr[C_1^{-1}\sum_{i=1}^{N} X_i X_i^*]\}}{\pi^{Np}|C_1|^N}\frac{exp\{-tr[C_2^{-1}\sum_{i=N+1}^{2N} X_i X_i^*]\}}{\pi^{Np}|C_2|^N} \tag{15}$$

Substituting into equation 15, we arrive at

$$lrt = \frac{\pi^{-2Np}|C_1|^{-2N}exp\{-tr[C_1^{-1}\sum_{i=1}^{2N} X_i X_i^*]\}}{(\pi^{-2Np}|C_1|^{-N}exp\{-tr[C_1^{-1}\sum_{i=1}^{N} X_i X_i^*]\})(\pi^{-Np}|C_2|^{-N}exp\{-tr[C_2^{-1}\sum_{i=N+1}^{2N} X_i X_i^*]\})} \tag{16}$$

Further, under the Null hypothesis "H_0", the maximum likelihood estimate of the unknown covariance C_1 is

$$C_1 = \frac{1}{2N}\sum_{i=1}^{2N} X_i X_i^*,$$

and under the alternative hypothesis "H_1", the maximum likelihood estimate of the unknown covariance matrices C_1 and C_2 are

$$C_1 = \frac{1}{N}\sum_{i=1}^{N} X_i X_i^*, \qquad C_2 = \frac{1}{N}\sum_{i=N+1}^{2N} X_i X_i^*.$$

Finally, with the substitution of unknown covariance matrices, we arrive at the simplified form of the generalized likelihood ratio test:

$$glrt = \frac{|\frac{1}{N}\sum_{i=1}^{N} X_i X_i^*|^N |\frac{1}{N}\sum_{i=N+1}^{2N} X_i X_i^*|^N}{|\frac{1}{2}(\frac{1}{N}\sum_{i=1}^{N} X_i X_i^* + \frac{1}{N}\sum_{i=N+1}^{2N} X_i X_i^*)|^{2N}} \tag{17}$$

The test detects of whether a change has occurred. Specifically, when the sample covariance matrices of time one and time two data are equal, i.e., when a change has *not* occured, then $C_1 = C_2 = \frac{1}{N}\sum_{i=1}^{N} X_i X_i^* = \frac{1}{N}\sum_{i=N+1}^{2N} X_i X_i^*$ and $glrt = 1$. By contrast, when the sample covariance matrices are not equal, implying a change has occurred, we obtain the result $0 \leq glrt \leq 1$.

This test is easily extended to multiple passes for more than two time specific images.

Specifically with M measurements, the generalized likelihood ratio test is

$$glrt = \frac{|\frac{1}{N}\sum_{i=1}^{N} X_i X_i^*|^N |\frac{1}{N}\sum_{i=N+1}^{2N} X_i X_i^*|^N \ldots, |\frac{1}{N}\sum_{i=(M-1)N+1}^{MN} X_i X_i^*|^N}{|\frac{1}{M}(\frac{1}{N}\sum_{i=1}^{N} X_i X_i^* + \frac{1}{N}\sum_{i=N+1}^{2N} X_i X_i^*, \ldots, +\frac{1}{N}\sum_{i=(M-1)N+1}^{MN} X_i X_i^*)|^{MN}} \tag{18}$$

and is used in our method to evaluate change statistically.

3.3 Overall Algorithm

Algorithm 1 provides the steps for obtaining the change characteristic γ. Then, based on some user prescribed threshold τ, we say that a change occurs at a given pixel for $\gamma > \tau$. We assume that there may be multiple passes at each measurement time. To this end, we let J be the total number of measurements and let J' be the number of "unchanged" measurements.

Algorithm 1 Change statistic algorithm given Fourier data at two different times

Input: Fourier data for J' measurements at time one and $J - J'$ measurements at time two.

1. **Compute Concentration Factor:** Compute exponential concentration factors according to size of input with $\sigma_E(\eta) = C\eta e^{(\frac{1}{\alpha\eta(\eta-1)})}$ and set the order $\alpha = 16$, where C is the normalizing constant defined as $C = \frac{\pi}{\int_{1/N}^{1-1/N} exp(\frac{1}{\alpha\tau(\tau-1)}d\tau)}$
2. **Obtain Edge Map:** Compute partial sum approximation of the jump function with concentration factors.
3. **Change Detection:** Using Edge masks $E_1, \ldots E_J$ as inputs, apply glrt on the multi-measurement data.

Output: change characteristics $\gamma \in [0, 1]$

3.4 Optimization of Concentration Factors

Another improvement we seek on the overall algorithm is to take advantage of the information of which Fourier data bands are incomplete. From the work done in [10], extended to 2D, the following procedures are developed. From our previous discussion of the jump response in section 3.1, we revisit the definition for a jump response in definition 3.4. A higher derivative jump response is extended with the below definition:

Definition 3.5. The first derivative jump response $W_1^{\sigma,N}(x)$ is

$$W_1^{\sigma,N}(x) = \frac{1}{2\pi} \sum_{0<|k|\leq N} \frac{\sigma(\frac{|k|}{N}}{ik^2} e^{ikx} \tag{19}$$

and in general,

$$W_q^{\sigma,N}(x) = \frac{1}{2\pi} \sum_{0<|k|\leq N} \frac{\sigma(\frac{|k|}{N}}{i^q k^{q+1}} e^{ikx} \tag{20}$$

We can then recompose the partial sum approximation

$$S_N^{\sigma}[f](x) = [f](\xi)W_0^{\sigma,N}(x-\xi) + [f'](\xi)W_1^{\sigma,N}(x-\xi) + [f''](\xi)W_2^{\sigma,N}(x-\xi) + \dots \tag{21}$$

The objective is to emphasize $W_0^{\sigma}(x)$ while suppressing the impact of each of the following higher derivative jump responses, $W_i^{\sigma}(x)$, $i = 1, 2, \dots$. Therefore, the design framework becomes solving an iterative program which computes a concentration factor such that conditions in section 3.1 are satisfied. The additional spurious responses from the missing Fourier data bands can lead to false jump detects, especially in the presence of noise. We can use the design framework to explicitly specify the missing data as a constraint in the problem formulation.

Therefore, the problem now becomes a convex optimization problem. We can constrain the jump response to be small beyond the immediate vicinity of the jump. i.e.

$$min_{\sigma} ||W_0^{\sigma,N}||_2$$

$$\text{subject to } W_0^{\sigma,N}|_{x=0} = 1$$

$$\sigma(K) = 0$$

$$|W_0^{\sigma,N}|_{|x|\geq 0.2} \leq 10^{-4}$$

where K is the missing Fourier bands. This new design process allows the concentration factor conditions to remain intact in case of missing data. The result is achieved through an optimization problem conducted through CVX programs in MATLAB.

4 Numerical results

4.1 Experiment Set Up

In addition to the preliminary experiments we conducted, the possible addition of noise needs to be considered in further experimentation. We are now ready to demonstrate numerical experiment results of our algorithm shown in algorithm 1. We first discuss how Fourier data is acquired. As shown in figure 8 , let F_j with resolution N be the Fourier domain signal of f_j, representing the j^{th} image. The signal is in the form of a single measurement vector $F_j = [F_{j1}, \ldots, F_{jN}]$. By the techniques described in [11], we first over sample F_j, satisfying the sampling rate described by the sampling theorem. Then a discrete Fourier transform implemented through FFT is applied to obtain signals in the Fourier domain. It's common that when Fourier data is sampled from devices, noise of varying degree will be present due to equipment degradation and other unavoidable factors. To set up such parameters, noise is added to the measurements in the Fourier domain. We tested our method on problems with various signal to noise ratio (SNR), where SNR is defined as

Definition 4.1 (Signal to Noise Ratio)**.** The SNR of the jth image is

$$SNR_{dB_j} = 10 \log_{10}(\frac{\hat{f}_j}{\sigma_j})^2$$

where $\hat{f}_j$ is the expected value of the input image in the spatial domain and σ_j is the variance of a normally distributed random variable $N(0, \sigma_j^2)$

For our numerical experiments we first choose the SNR for each of the $j = 1, \ldots, J$ images, and then back-calculate the corresponding variance of the random variable yielding the measurement of the form $Y_j = F_j + \epsilon$, where $\epsilon \sim N(0, \sigma_j^2)$ for image j. Lastly, we achieve our goal of mimicking under-sample data by zeroing our Fourier frequency bands as described in 1. As already noted above, our data set has J images in total, and J' of those images are reference images while the remaining $J - J'$ images are changed. Experiments are run on a SAR image of a golf course as shown below:

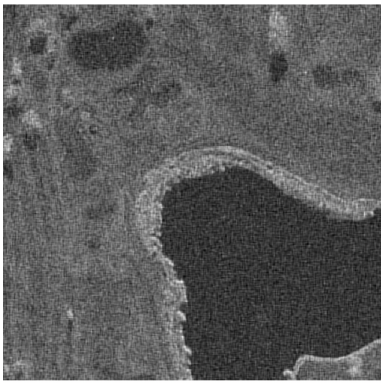

Figure 8: Underlying Scene

We proceed to create changed scenes as well as fitting into the data described above for three referenced and three changed scenes.

4.2 Experiment Evaluation

To evaluate our results, a receiver operating characteristic (ROC) curve is calculated for each change characteristic. This curve illustrates the diagnostic ability of our algorithm to correctly classify change and no change. The plots are created by plotting the true positive rate (TPR) against the false positive rate (FPR) at various threshold settings. An ideal change detector would shown a vertical straight line at $x = 0$ connected with horizontal straight line at $y = 1$ while a true random change detector would display a diagonal line with slope equals to 1. More details of how ROC curves can be applied to evaluate classifiers can be found in [7].

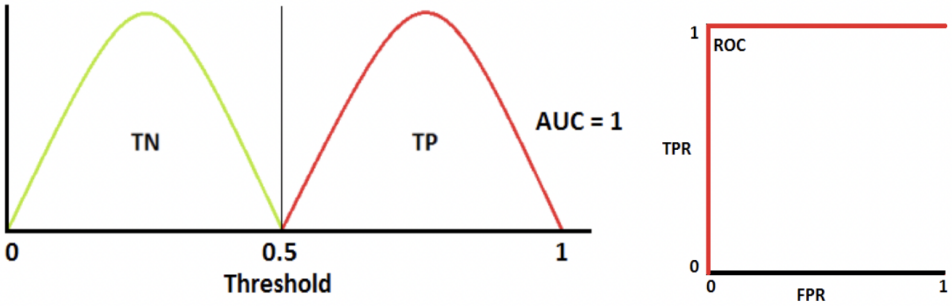

Figure 9: Example of ROC Curve: Perfect Classifier

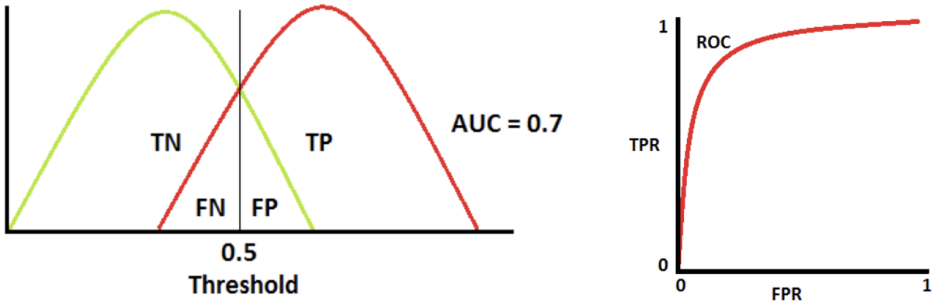

Figure 10: Example of ROC Curve: Un-perfect Classifier

As shown in the examples above, the first classifier is able fully distinguish between true positive cases and true negative cases, making it a perfect classifier with its corresponding ROC curve. The second classifier has some false negative and false positive detection, decreasing its area under the curve for the corresponding ROC curve.

And lastly, we evaluate all of our experiments against an inverse Fourier reconstruction as the bench mark. We are interested to see what's the margin of improvements on our process. A result of same or better is desired in cases of under-sampled data. We remap the received frequency data Y into in spatial domain. The GLRT algorithm then calculates the change statistics of two sets of images. The result, γ, is the change statistics of a data set, $\gamma : [-1, 1]^2 \to [0, 1]$ where $\gamma = 0$ if there is no change and $\gamma = 1$ if there is a change.

4.3 Experiment 1: Different Bands

We are now ready to demonstrate the results using the concentration factor method. In these cases, when the images are converted into Fourier domain, certain bands of Fourier data are masked with zeros. Further, different bands are blocked out for signals at different times. Figure 11 shows the Fourier reconstruction of the image with $SNR = 10$ dB.

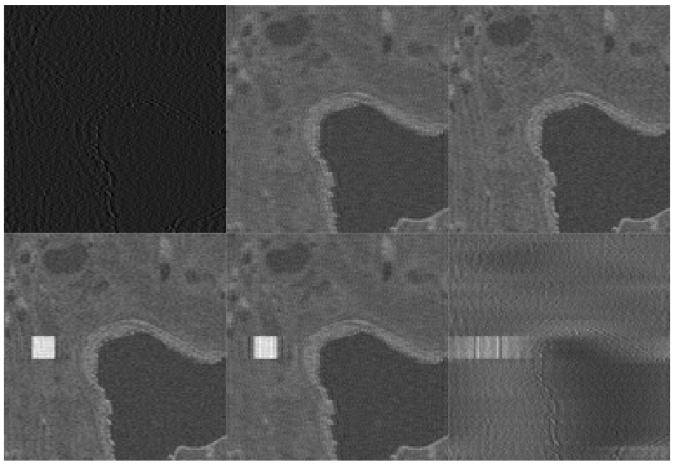

Figure 11: Fourier Reconstruction of Under-sampled Data. Here $SNR = 10$ dB.

The band which signals are zero-filled has a width of 15 pixels, and the bands are laid in horizontal direction to mask phase information. Figure 12a shows the change detection GLRT using the test statistic on the standard Fourier reconstruction. The ROC curve shows that the test statistic is not very effective at discerning the change.

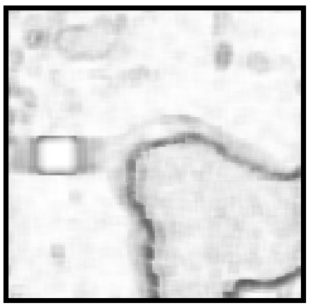

(a) Change Detection for Standard Fourier Reconstruction Recovery

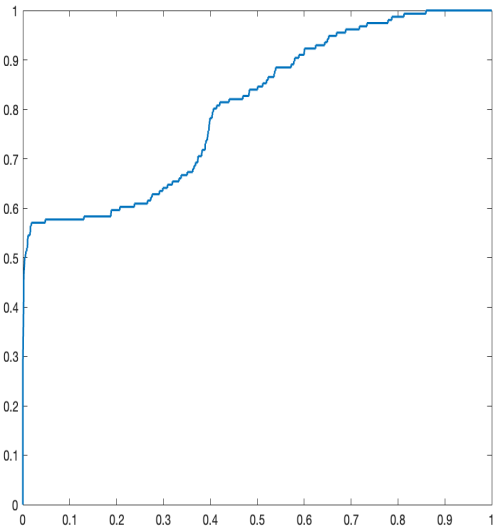

(b) ROC Curve for Inverse Fourier

Figure 12: SNR = 10, Under Sample Band Width = 15

We now apply our algorithm, which computes an edge map for the under-sampled Fourier

data. GLRT is then applied onto the edge maps The results of GLRT as well as the ROC curve are displayed in Figure 13.

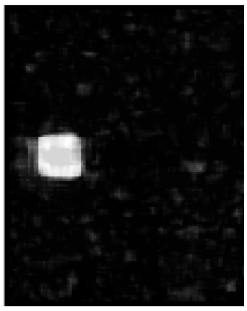

(a) Change Characteristics for Edge Map

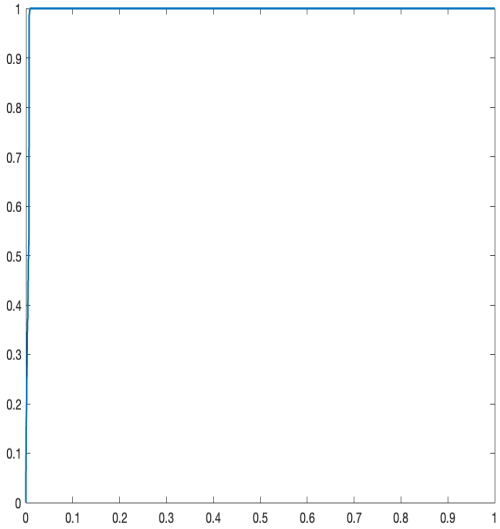

(b) ROC Curve for Edge Map

Figure 13: SNR = 10, Under sample band width = 15

As demonstrated in Figure 13, pre-processing with an edge map allows change detection to differentiate between "damaged" data, and data with full Fourier bands, keeping the GLRT results intact. However, when using the standard Fourier reconstruction, the algorithm takes in these blurry reconstructions to detect changes as well, resulting in non-robust results. Figures 14 and 15 compare the ROC curves of results of our method with using the standard Fourier recovery method for SNR ranging from $-5dB$ to $25dB$, with a $5dB$ increment.

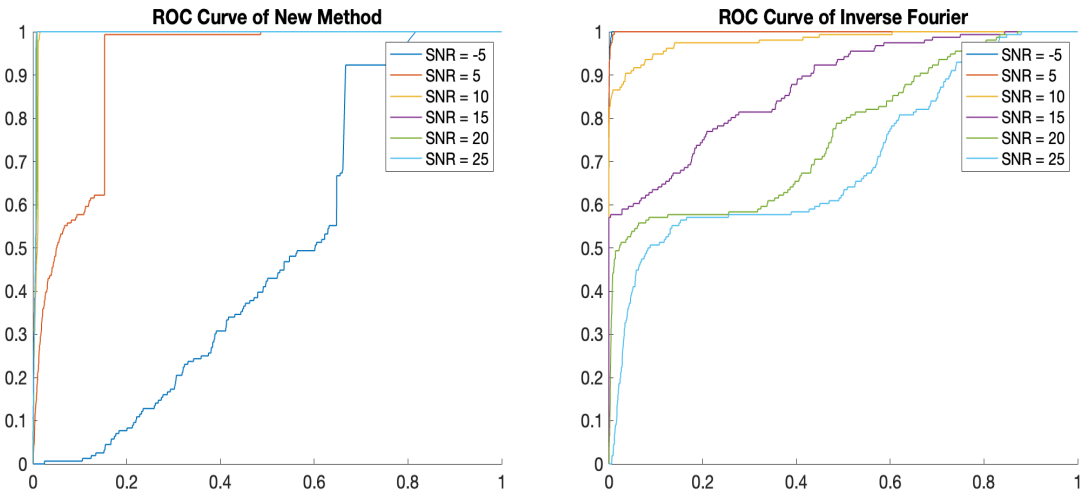

(a) ROC Curve for new method (b) ROC Curve for Inverse Fourier

Figure 14: Ranging from SNR = [-5,5,10,15,20,25]

Observe that for an $SNR \geq 10$, using the edge map instead of the standard Fourier reconstruction yields better accuracy when determining change. On the other hand, our method does not work well for very low SNRs.

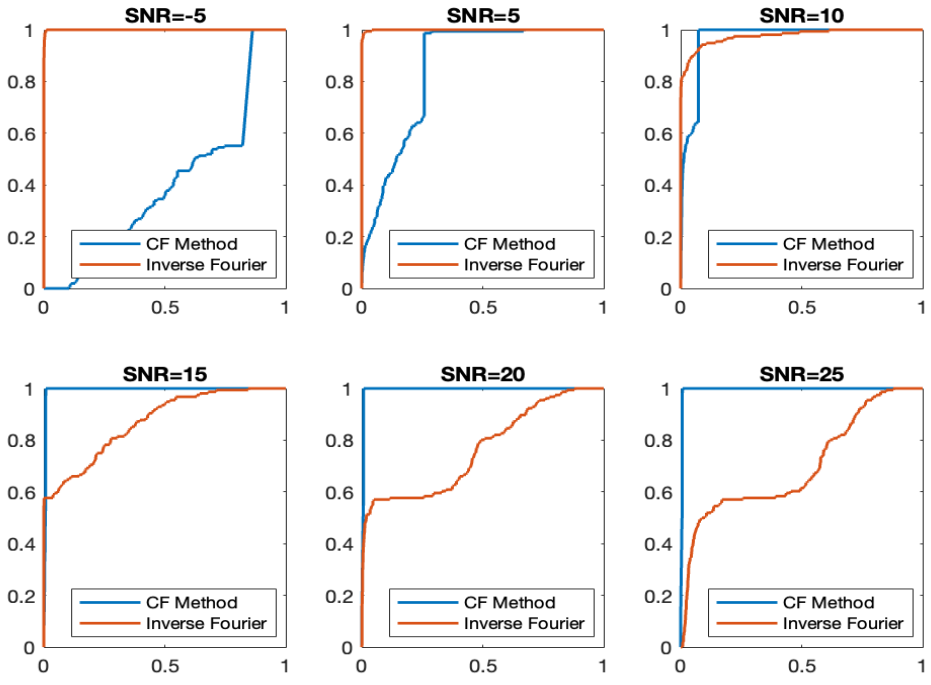

Figure 15: Inverse Fourier VS CF Method across SNR

It is surprising that using standard Fourier reconstruction performs well at low SNR, indeed better than its performance at higher SNR. Future work is needed to understand this result.

4.4 Experiment 2: Bands with Noise

In a more realistic setting, it's more likely that the Fourier bands in which the signals are interfered with will be replaced with noise. In contrast to the previous experiments where these Fourier bands are simply zeroed out, another numerical experiment is conducted. In this case, the identified missing Fourier bands are replaced with values randomly sampled from a normal distribution. The variance of such normal distribution corresponds to the SNR of the overall experiment. Figure 16 shows an inverse Fourier reconstruction for this example.

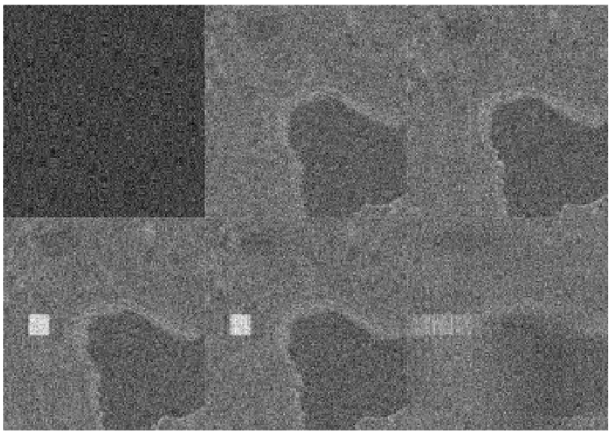

Figure 16: inverse Fourier reconstruction of Fourier Data, SNR = 5

Due to the fact that high frequency Fourier signals are completely replaced by noise, the reconstruction of scene one barely has any identifiable features while scene two through four remained largely intact. Figure 17a shows the ROC curves of results of our method versus using an inverse Fourier method with SNR ranging from $-5dB$ to $25dB$, with a $5dB$ increment.

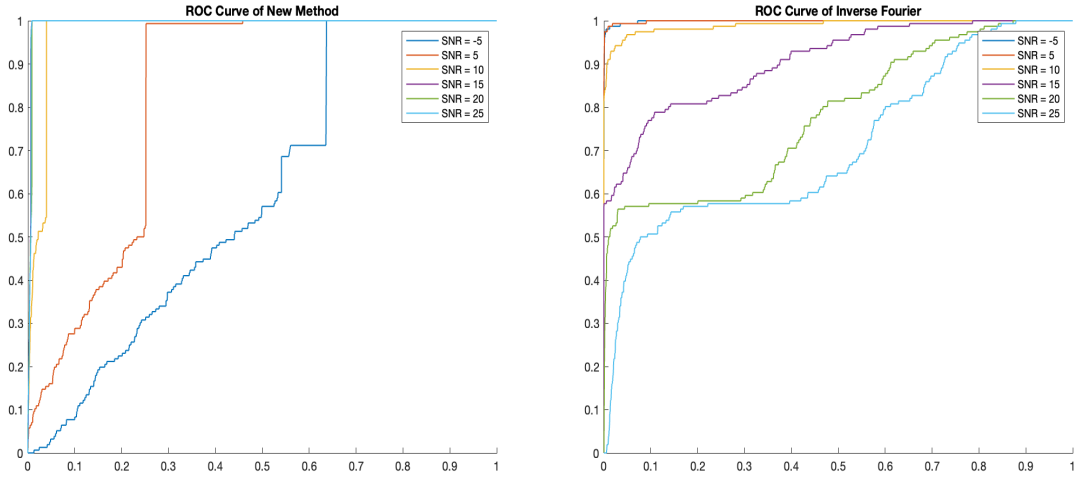

(a) ROC Curve for CF method (b) ROC Curve for Inverse Fourier

Figure 17: Ranging from SNR = [-5,5,10,15,20,25]

We can see overall that our method yields a more robust result with greater areas under the curve for the ROC curves.

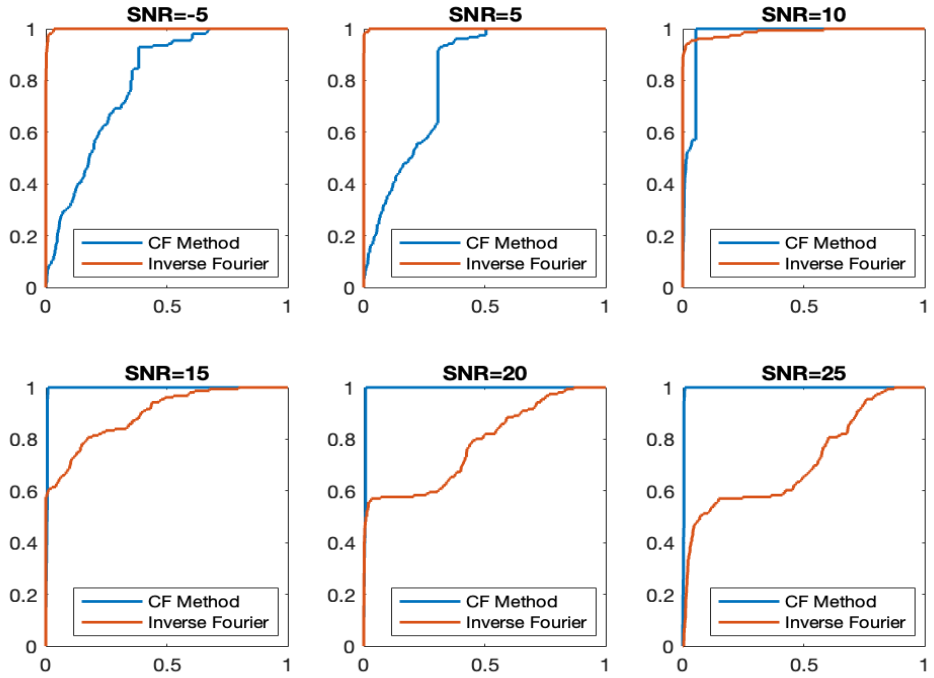

Figure 18: Inverse Fourier VS CF Method across SNR

We see a small change in the results we obtain in figure 18. Both methods now delivers

slightly worse performance at lower SNR, or higher noise. This fits out intuition as the higher SNR, the more noise there will be in the originally zeroed Fourier bands, causing a decrease in quality of reconstruction. However, we see the general trends from the previous experiment continue, at higher SNR, the new pre-processing method delivers better result than simply doing an inverse Fourier reconstruction.

4.5 Experiment 3: Same Bands

The next numerical experiment we consider is the case in which we under-sample the same Fourier bands for every scene we obtain. Two situations are considered: when the high frequency signals are interfered with and when the low frequency signals are interfered with. Since each Fourier coefficient is embedded with different information, we want to see the result of such an algorithm in both situations.

4.5.1 Experiment 3.1: High Frequency Bands

First consider the experiment where high frequency bands are zeroed-out. We zeroed out both low frequency and high frequency signals and replaced them with noise of respective SNR.

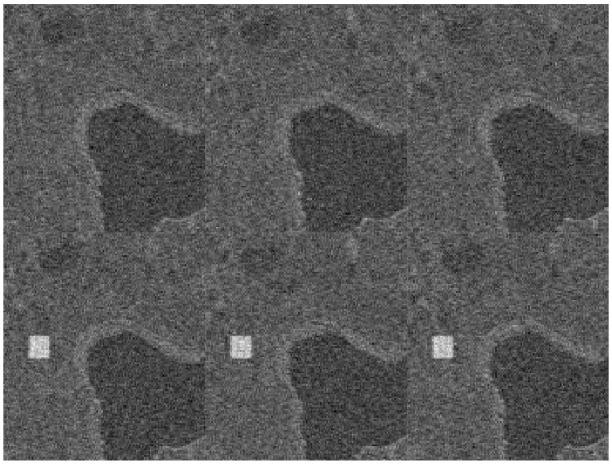

Figure 19: inverse Fourier reconstruction of Fourier data, SNR = 5

As we can see in figure 19, in this experiment, the compromised signals had the least effect on reconstruction qualities of images by inverse Fourier transform. As a result, one can

reasonably assume that inverse Fourier would have a robust performance. We are curious to see how the quality of our method compares against the benchmark of Fourier transform.

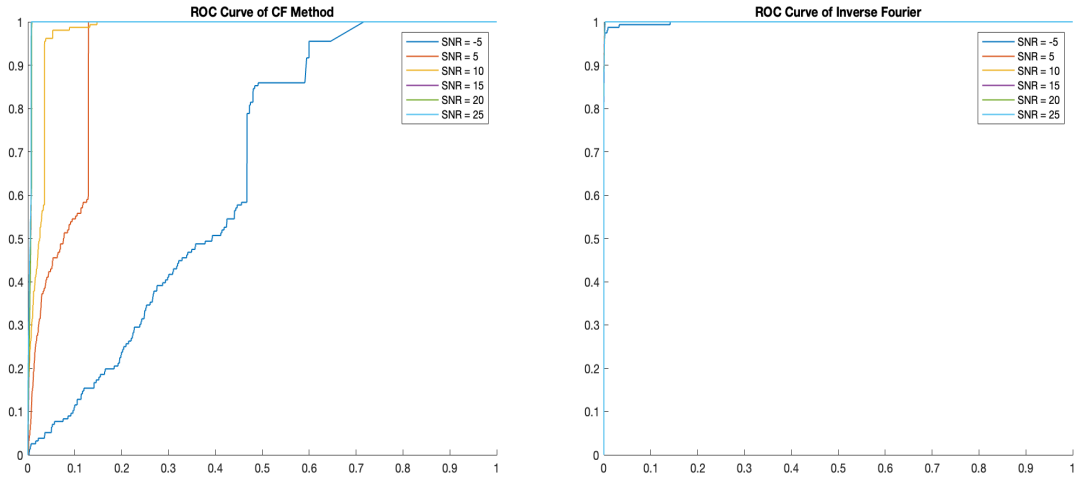

(a) ROC Curve for CF Method

(b) ROC Curve for Inverse Fourier

Figure 20: Ranging from SNR = [-5, 5,10,15,20,25]

Both our method and the bench mark have improved performance in change detection. Inverse Fourier had a drastic increase in accuracy from both a decrease in false negative and false positive across all SNR. Although the CF method doesn't show as robust of a result as inverse Fourier in high noise environments, it performed as well in low noise experiments.

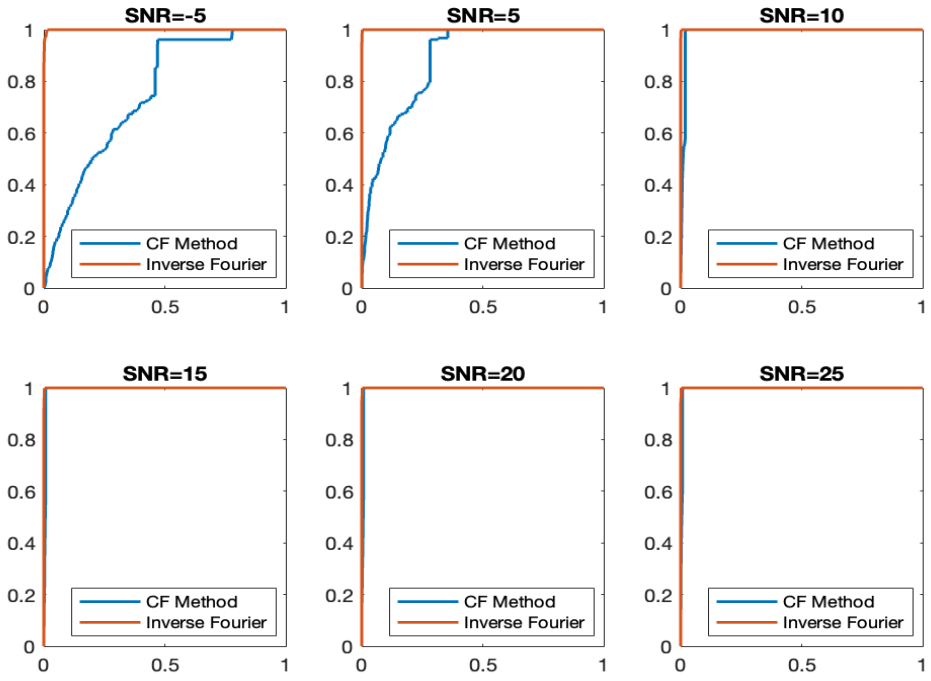

Figure 21: Inverse Fourier VS CF Method across SNR

4.5.2 Experiment 3.2: Low Frequency Bands

Now in parallel, we are interested in the results of low frequency band interferences. These experiments will be the most difficult to obtain a robust result from. The low frequency signals contain more "information" about the images. Since those signals are interfered with, the image reconstruction "lost" most of its features. The following image shows a reconstruction with inverse Fourier transform.

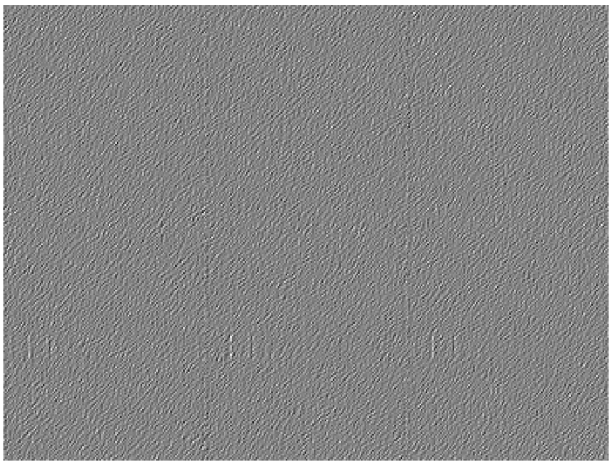

Figure 22: inverse Fourier reconstruction of Fourier data, SNR = 5

The experiment was conducted with SNR = 5. One can follow the intuition and conjecture that the results from both inverse Fourier transform and the new methods would have decrease accuracy, as shown below:

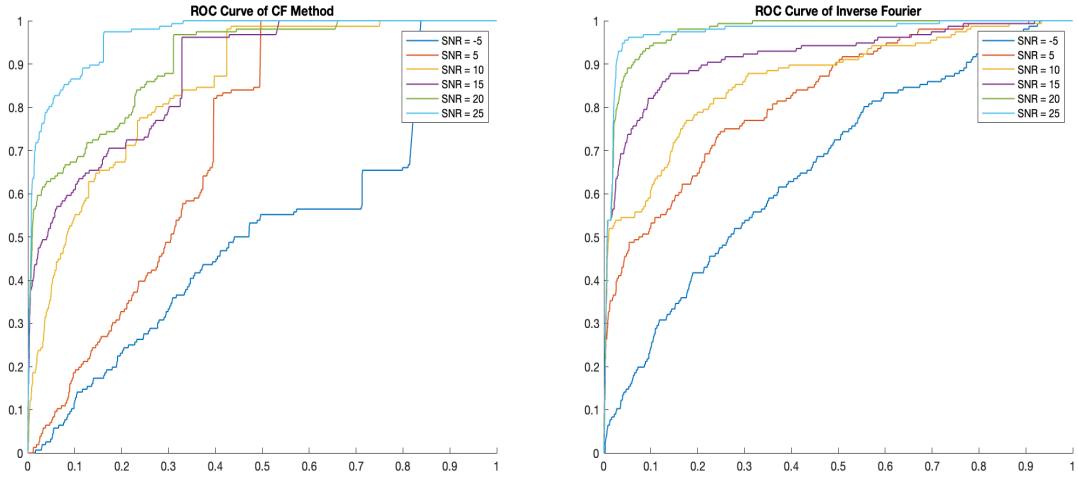

(a) ROC Curve for New Method (b) ROC Curve for Inverse Fourier

Figure 23: Ranging from SNR = [5,10,15,20,25]

Across both methods, we see a decrease in accuracy, especially in high noise environments. Also across both methods, we do not see an almost perfect ROC curve for low noise cases. We can see from the results in figure 24 below that the low frequency bands interference impact the new methods at low noise environments, but actually increased accuracy of inverse

Fourier methods at low noise experiment. Due to the extrapolation of low frequency coefficients, missing frequency bands actually decrease the number of false positives exhibited by the ROC curves.

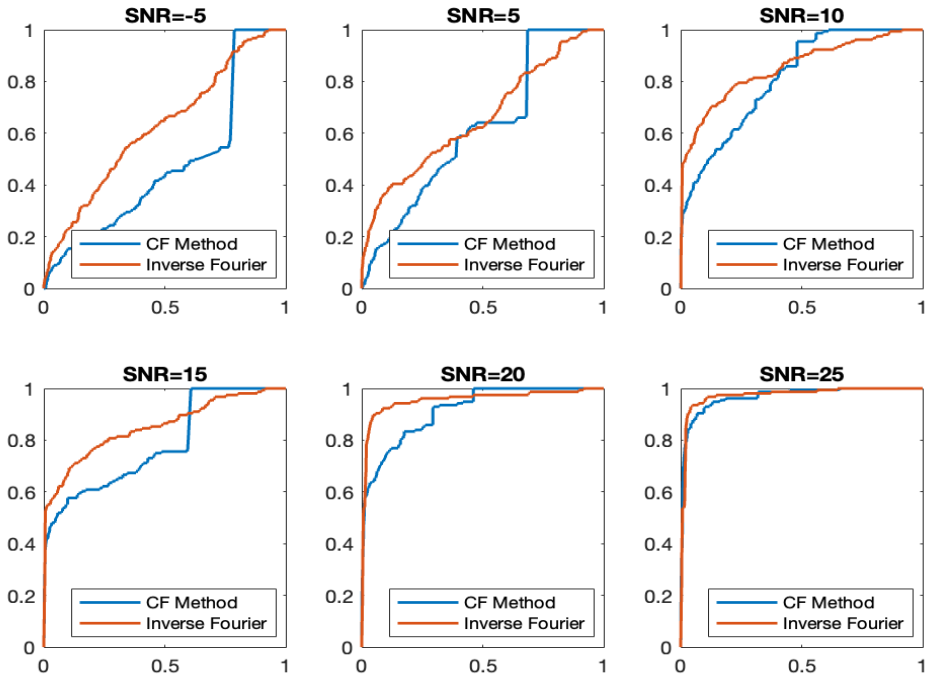

Figure 24: Inverse Fourier VS CF Method across SNR

4.6 Optimized Concentration Factor Method

With methods described in section 3.4, we evolve our method further to improve its accuracy, taking advantage of the fact that we know what frequency bands are missing. We want to see how the method performs against both the existing method and inverse Fourier transform. Numerical experiments are conducted with the optimized CF method. First we consider under-sampling different Fourier bands for each scene.

4.7 Experiment 4: Different Bands

With the method described in section 3.4, below is a reconstruction of each scene along with the corresponding concentration factors we have recovered.

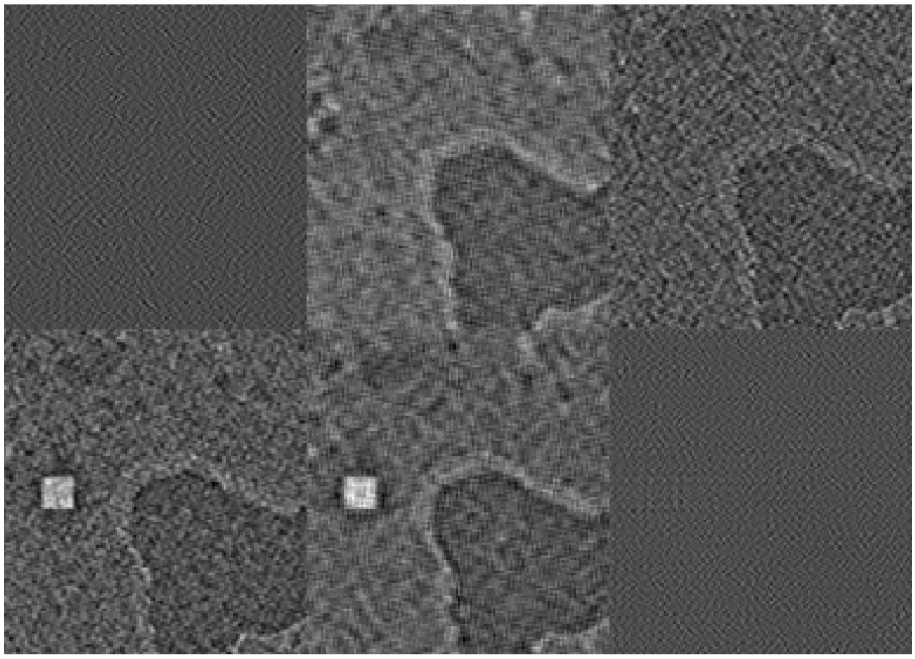

Figure 25: Golf Course Scenes Recovered from Optimized CF Method, SNR = 5

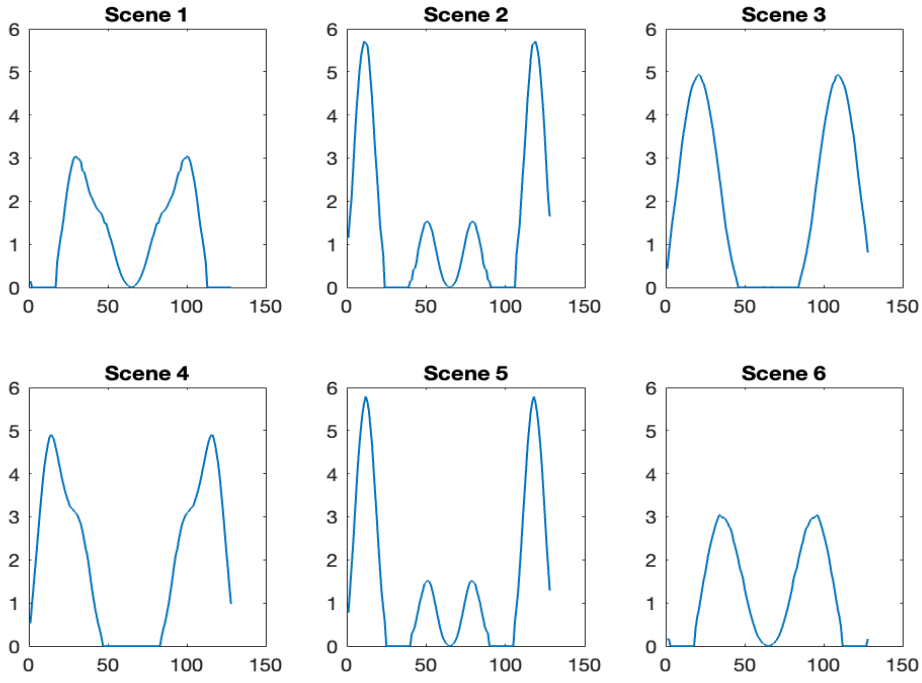

Figure 26: Concentration Factor from Optimized CF Method, SNR = 5

From the concentration factor constructed, we can see that the corresponding "missing" Fourier bands are set to zero, allowing the rest of the concentration factors to optimize.

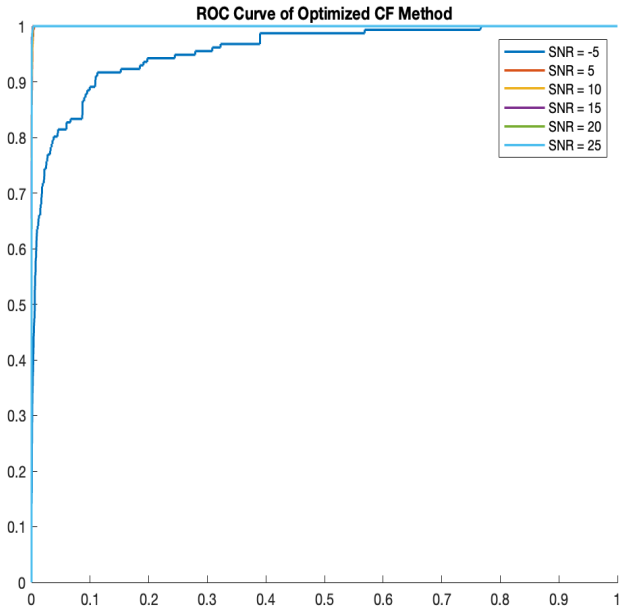

Figure 27: ROC Curve for Optimized CF method across SNR

Below we show the ROC curves of Optimized CF Method against the previous method. We can see there is an increase in accuracy across all SNRs, especially when noise is high. The optimized concentration factors allow us to obtain a more accurate edge map and thus a more robust result for change detection.

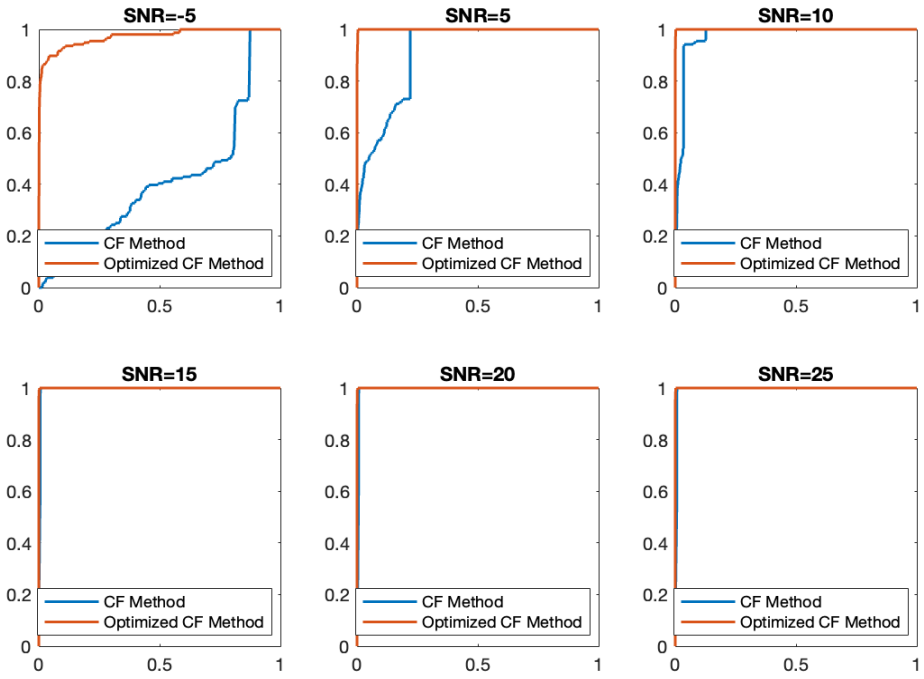

Figure 28: CF Method VS Optimized CF Method across SNR

4.8 Experiment 5: Same Band

Next, the optimized method is applied to experiments where low frequency Fourier data are missing. The low frequency bands are zeroed.

4.8.1 Experiment 5.1: High Frequency Bands

We then explore the case where high frequency bands are missing. Again, below we see a reconstruction with optimized concentration factor method with high frequency bands zeroed out. We see a high reconstruction quality, align with the fact that high frequency bands carry less information. We also show the calculated concentration factors for each scene, incorporating the fact that we are missing the high frequency bands; the factors in the middle are zeroed out.

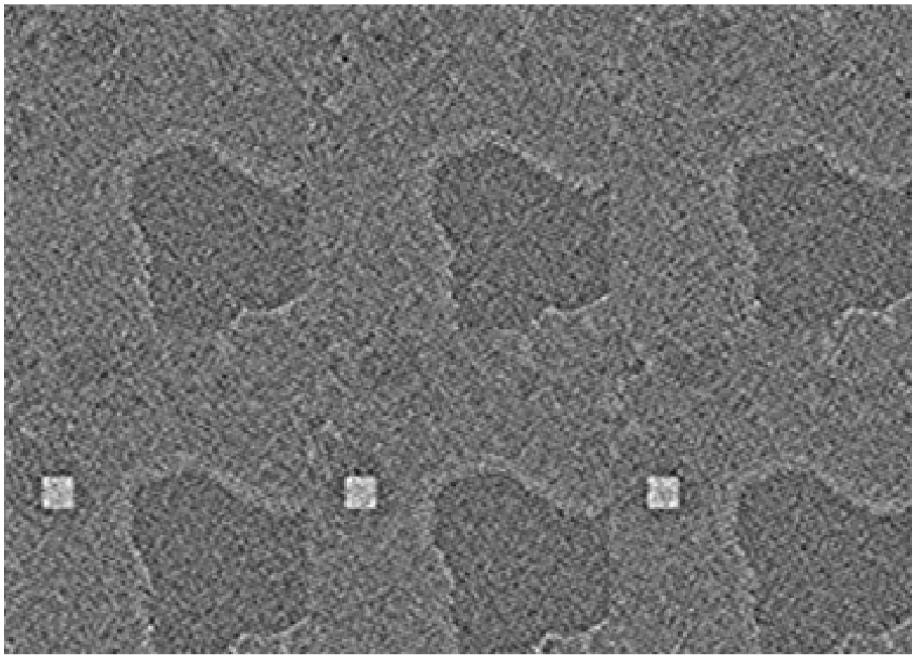

Figure 29: Golf Course Scene Recovered from Optimized CF Method, SNR = 5

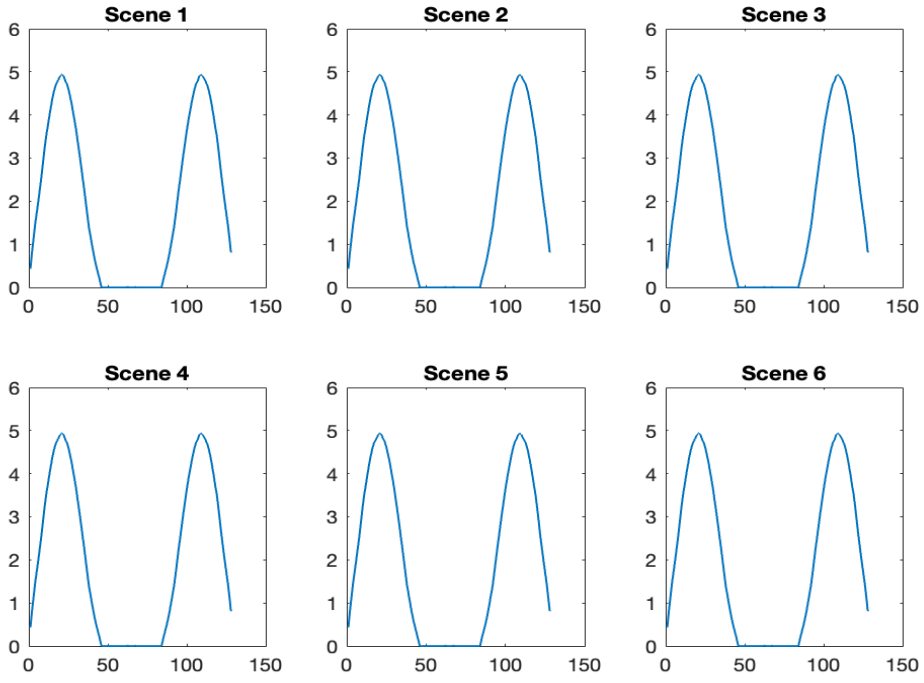

Figure 30: Optimized CF Method Concentration Factor Weights across Scenes

The ROC curve of the Optimized CF method shows a general robustness in the method. We also show comparisons between CF and Optimized CF method across SNR below, the Optimized CF method shows a much more even performance, especially exceeding regular CF method when noise present is high.

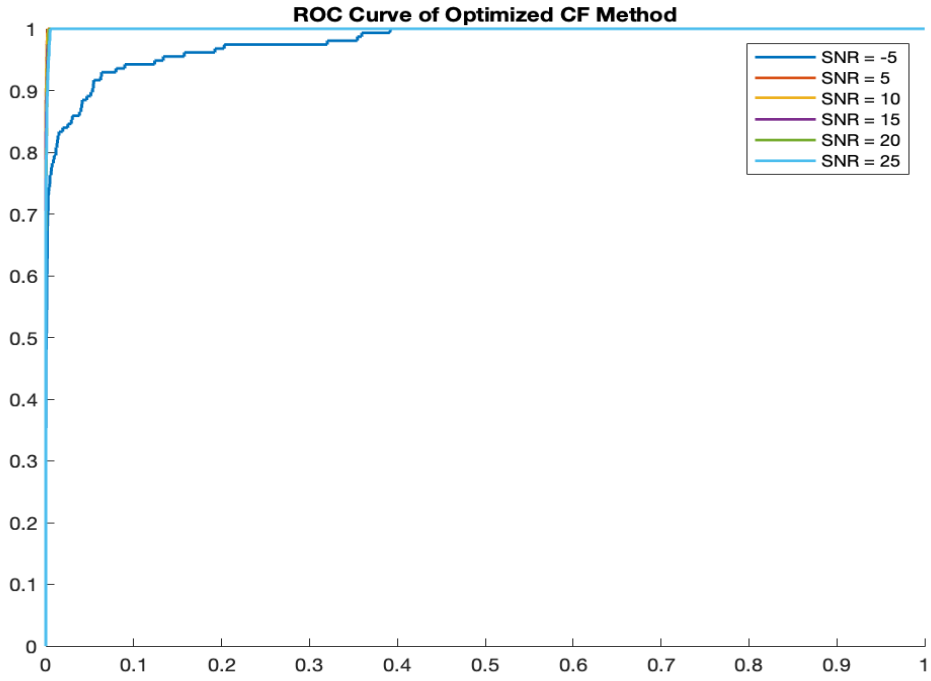

Figure 31: Optimized CF Method across SNR

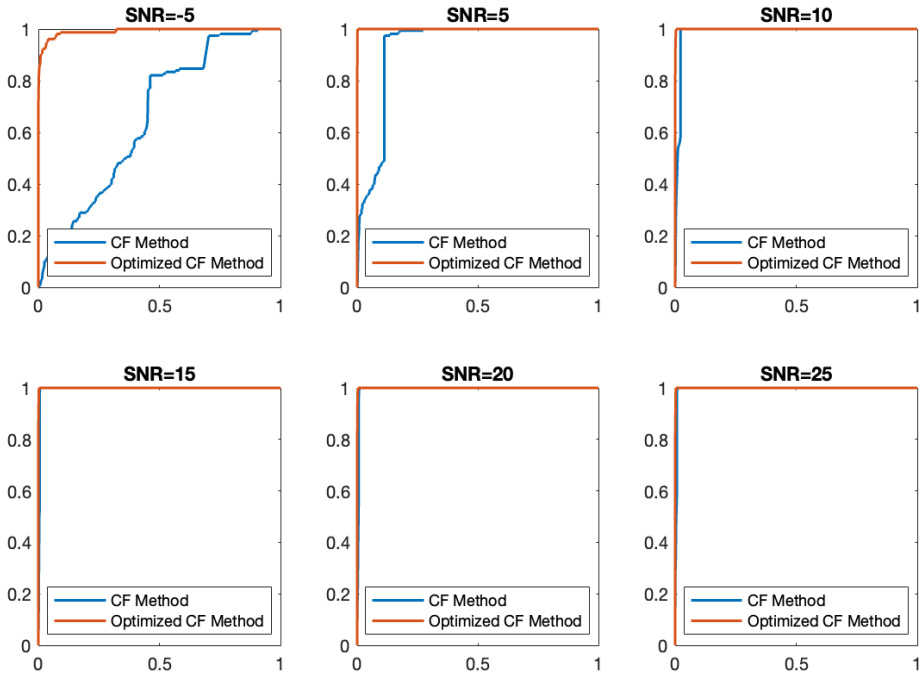

Figure 32: CF Method VS Optimized CF Method across SNR

4.8.2 Experiment 5.2: Low Frequency Bands

Now we are interested in how the method performs in scenarios where low frequency bands are missing. In such cases, both the CF method and Inverse Fourier have performed poorly comparing to other scenarios. This is the most challenging case, as we are missing the most information these Fourier data are able to provide us. As seen in the following figure, we have the new optimized concentration factors, taking into account the fact the high frequency Fourier data bands are missing.

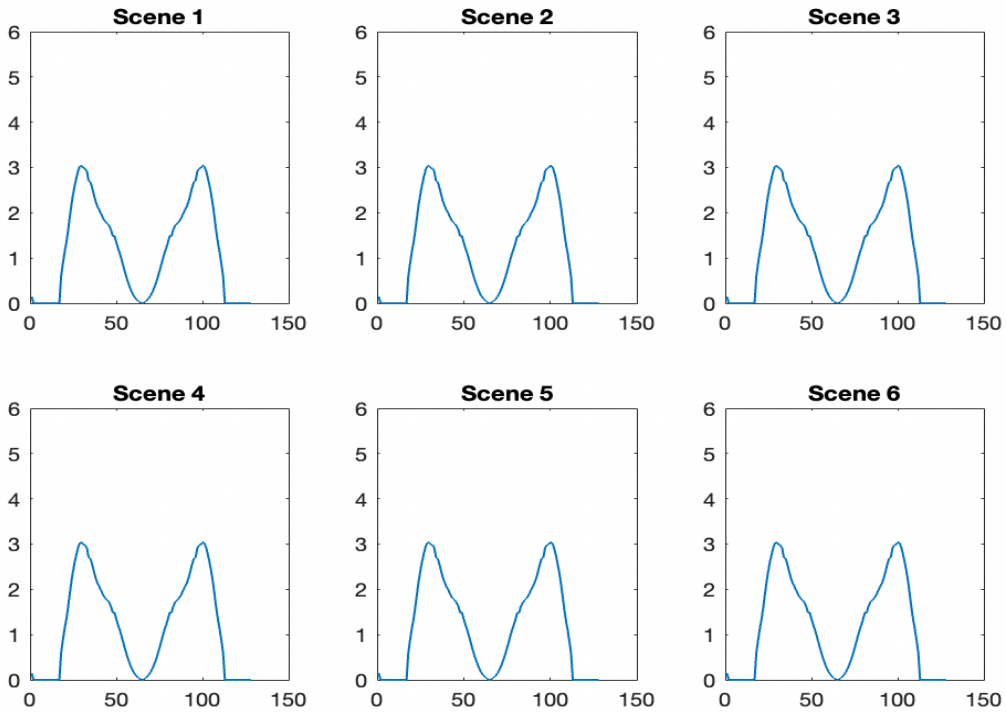

Figure 33: CF Method VS Optimized CF Method across SNR

With these, we are able to conduct numerical experiments across SNRs to compare the results with both inverse Fourier transform as well as the CF method.

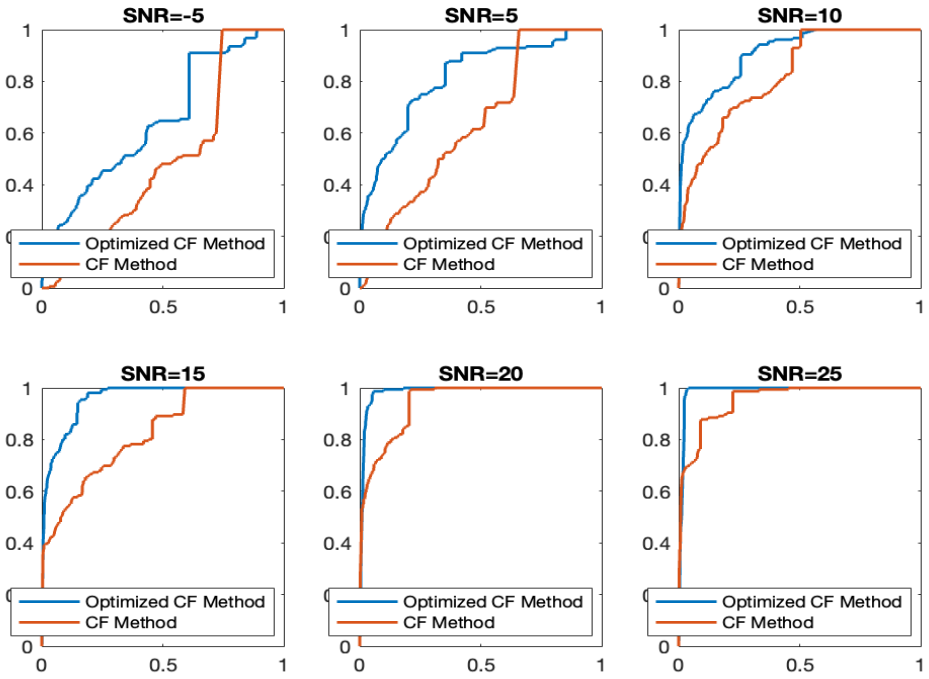

Figure 34: CF Method VS Optimized CF Method across SNR

We see an improvement in both the sensitivity and specificity of the method. The Optimized method performs better than our original CF method in this case across all noise levels. More importantly, as shown below, we see an improvement in robustness across all SNRs when our optimized method is compared with inverse Fourier transform.

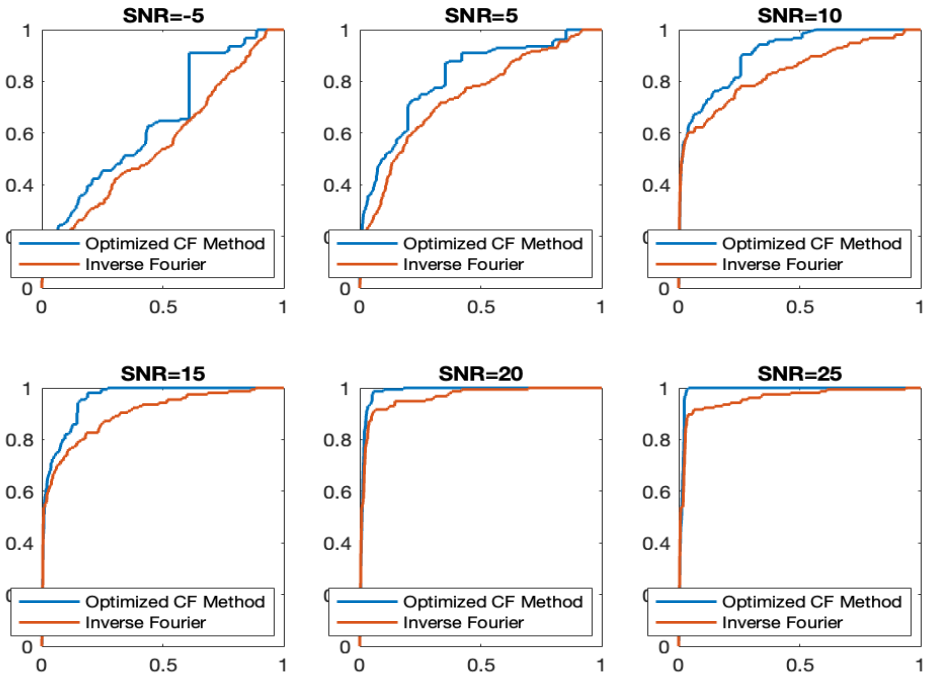

Figure 35: CF Method VS Optimized CF Method across SNR

Further, we see a marginal increase in the computational power required by our optimized method. Although, an optimizing program is required to obtain the new concentration factor, knowing what bands are missing, the concentration factors are image independent. Therefore, we will be able to create such factors only knowing the size of our data, then apply such factors to the data obtained.

5 Concluding thoughts

5.1 Results Conclusion

We now want to conclude the effects of different methods for the different experiments conducted. Although the ROC curves provides us with a great insight of relative performance of methods, it becomes hard to quantitatively characterize these methods and see margins of improvements. Thus, we move on to calculate the area under the curve, or AUC of these methods. AUC provides an aggregated measure of performance of the method. AUC ranges from 0 to 1, with higher values being more desirable. As seen in the table below:

SNR	-5	5	10	15	20	25
Different Bands						
Inverse Fourier	0.999	0.999	0.977	0.871	0.765	0.703
CF	0.561	0.929	0.992	0.995	0.995	0.996
Optimized CF	0.999	0.999	0.999	0.999	0.999	0.999
Same Bands (Low Frequency)						
Inverse Fourier	0.998	0.999	0.999	0.999	0.999	0.999
CF	0.545	0.836	0.992	0.996	0.996	0.996
Optimized CF	0.983	0.999	0.999	0.999	0.999	0.999
Same Bands (High Frequency)						
Inverse Fourier	0.547	0.634	0.834	0.875	0.946	0.968
CF	0.516	0.684	0.739	0.872	0.855	0.971
Optimized CF	0.661	0.738	0.966	0.943	0.986	0.989

Table 1: Summary of Method Performance across SNR

The percent improvements in terms of area under the curve for these ROC curves are included in the following table for both methods compared against inverse Fourier.

SNR	-5	5	10	15	20	25
Different Bands						
CF	-43.9%	-7.1%	-0.7%	0%	0%	0%
Optimized CF	0%	0%	0%	0%	0%	0%
Same Bands (Low Frequency)						
CF	-45.3%	-16.3%	0%	0%	0%	0%
Optimized CF	-1.5%	0%	0%	0%	0%	0%
Same Bands (High Frequency)						
CF	-5.6%.	7.9%	-11.3%	0%	-9.6%	0%
Optimized CF	20.8%	16.4%	15.8%	7.7%	4.2%	2.1%

Table 2: Summary of Method Performance by Percentage across SNR

5.2 Research Discussions

The methods we employed have several advantages. Concentration factor is a very robust method that is widely used. These factors are image independent and only depend on the size of the images. These concentration factors could be saved and applied on Fourier signals, making the process more computationally efficient especially with large sized image and data set. Further, experiments conducted in this project required few parameters. Concentration factors allow us to by-pass a full reconstruction which becomes difficult in times of compromised data. With these premise, we note that we would desire the concentration factor method to be performing at the same accuracy or better than our bench mark Inverse Fourier. And We can see that from all experiments, the optimized CF method has performed to the same level or better than our bench mark, making it a more robust and efficient pre-processing for change detection. Comparison of our method and state of the art can be found in the process charts below.

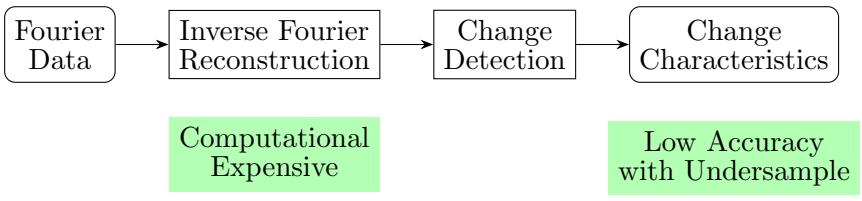

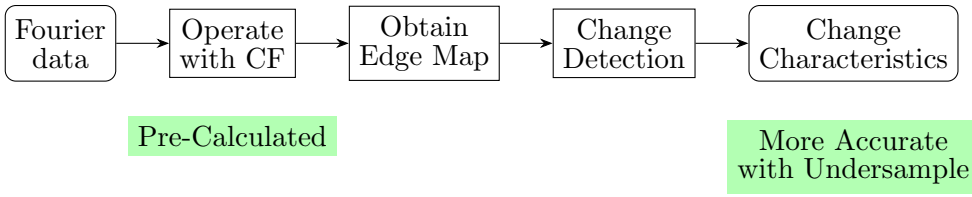

We now want to acknowledge areas of the method or the set of the experiments that are limited. The advantage of the optimized CF method is marginal in the low noise events when we conducted same bands experiments as well as high noise events with differentiating bands. In these cases, an inverse Fourier reconstruction performs with great accuracy. However, as noted in the above section, concentration factor operates with very little perimeter. Therefore, although the Optimized CF method performs at the same level as the benchmark, it is still the more advantageous method. In addition, although we are able to calculate concentration factors independent of input images, the optimized CF method does require optimization algorithms that will be computationally expensive with more Fourier coefficients required.

5.3 Future Work

There are limitations in the experiments that are have conducted as well. The biggest concern is that all numerical experiments are conducted on the same scene. Although the scene is a real-life captured SAR image, we wish to see the CF method's results on images with more features, or larger size images. Since concentration factor method is calculated with respect to the size of the images, this is the next most important perimeter we wish to vary. Aside from the underlying scene itself, we also wish to see the effects of more variations in ways which the data is under-sampled, with different width of frequency blockage or number of bands blocked out. We also want to extend experiments to larger images and bigger data sets. We are interested in the method's ability to maintain the accuracy advantage in under-sampled data in these larger scale problems.

We are also interested in how the pre-preocessing we have can extend to other change detection methods including online change detection or change detection with machine

learning methods. Lastly, we wish to extend the research into complex signals that more accurately simulate SAR image data or data fusion problem.

References

[1] Rick Archibald, Anne Gelb, and Jungho Yoon. Polynomial fitting for edge detection in irregularly sampled signals and images. *SIAM journal on numerical analysis*, 43(1):259–279, 2005.

[2] Albert Benveniste. *Advanced methods of change detection: An overview*. Springer Berlin Heidelberg, Berlin, Heidelberg, 1986.

[3] James W. Cooley, Peter A. W. Lewis, and Peter D. Welch. The fast fourier transform and its applications. *IEEE Transactions on Education*, 12(1):27–34, 1969.

[4] Shlomo Engelberg. Edge detection using fourier coefficients. *The American Mathematical Monthly*, 115(6):499–513, 2008.

[5] Anne Gelb and Taylor Hines. Detection of edges from nonuniform fourier data. *Journal of Fourier Analysis and Applications*, 17:1152–1179, 12 2011.

[6] Anne Gelb and Eitan Tadmor. Detection of edges in spectral data. *Applied and Computational Harmonic Analysis*, 7(1):101–135, 1999.

[7] Jayawant N. Mandrekar. Receiver operating characteristic curve in diagnostic test assessment. *Journal of Thoracic Oncology*, 5(9):1315–1316, 2010.

[8] Leslie M. Novak and Bae. Change detection for multipolarization , multi-pass sar. 2005.

[9] Wolfgang Stefan, Adityavikram Viswanathan, Anne Gelb, and Rosemary Renaut. Sparsity enforcing edge detection method for blurred and noisy fourier data. *J. Sci. Comput.*, 50:536–556, 03 2012.

[10] Adityavikram Viswanathan, Anne Gelb, and Douglas Cochran. Iterative design of concentration factors for jump detection. *Journal of Scientific Computing*, 51(3):631–649, June 2012. Funding Information: This work was supported in part by National Science Foundation grants CNS 0324957, DMS 0510813 and FRG 0652833.

[11] H. Joseph Weaver. *Theory of Discrete and Continuous Fourier Analysis*. John Wiley Sons, Inc., USA, 1989.

[12] P. M. Zwartjes and M. D. Sacchi. Fourier reconstruction of nonuniformly sampled, aliased seismic data. *GEOPHYSICS*, 72(1):V21–V32, 2007.